VORTEX FORMATION OVER DOUBLE-DELTA WINGS[+)]

U. Brennenstuhl[*]
D. Hummel[**]

Institut für Strömungsmechanik
Technische Universität Braunschweig
Federal Republic of Germany

Abstract

Low-speed wind-tunnel tests have been carried out on a series of double-delta wings. The effects of variations in leading-edge kink angle and in kink position have been investigated by means of three-component, pressure distribution and flow-field measurements as well as by flow visualization at Re = $1.3 \cdot 10^6$. At small angles of attack two primary vortices exist on each side of the wing, originating from the apex and from the leading-edge kink. At moderate kink angles these two vortices join each other with increasing angle of attack. The junction process is analysed in detail and is interpreted as a "potential flow effect". At very large angles of attack vortex breakdown occurs within the joined vortices, which leads to the limitations of the aerodynamic coefficients.

1. Introduction

On slender wings the flow separates from the sharp leading-edges at moderate and large angles of attack. These flow separations usually take the form of two spiral shaped vortex sheets joined to the leading-edge and rolling up into two primary vortices above the upper surface of the wing as sketched in Fig.1. The two vortices induce additional velocities at the upper surface of the wing and the corresponding pressure distribution shows distinctly marked minima beneath the vortex axes. Accordingly an additional lift force occurs which depends non-linearly on the angle of attack. Due to the leading-edge vortices the flow at the wing surface is directed outwards and passes a pressure gradient which causes additional flow separations in the form of small secondary vortices. The corresponding modification of the pressure distribution is also indicated in Fig.1. At very large angles of attack vortex breakdown takes place within the primary vortices. With increasing angle of attack these vortices are destroyed more and more and it is this effect which limits the aerodynamic coefficients.

This vortex formation is well known since a long time and various reviews on this subject have been published from time to time for instance by D. Küchemann [1], J.H.B. Smith [2] and D.J. Peake [3]. For a simple delta wing subsequent investigations by D. Hummel [4] led to the knowledge that the vortex sheet behind a slender wing rolls up into a concentrated trailing vortex the rotation

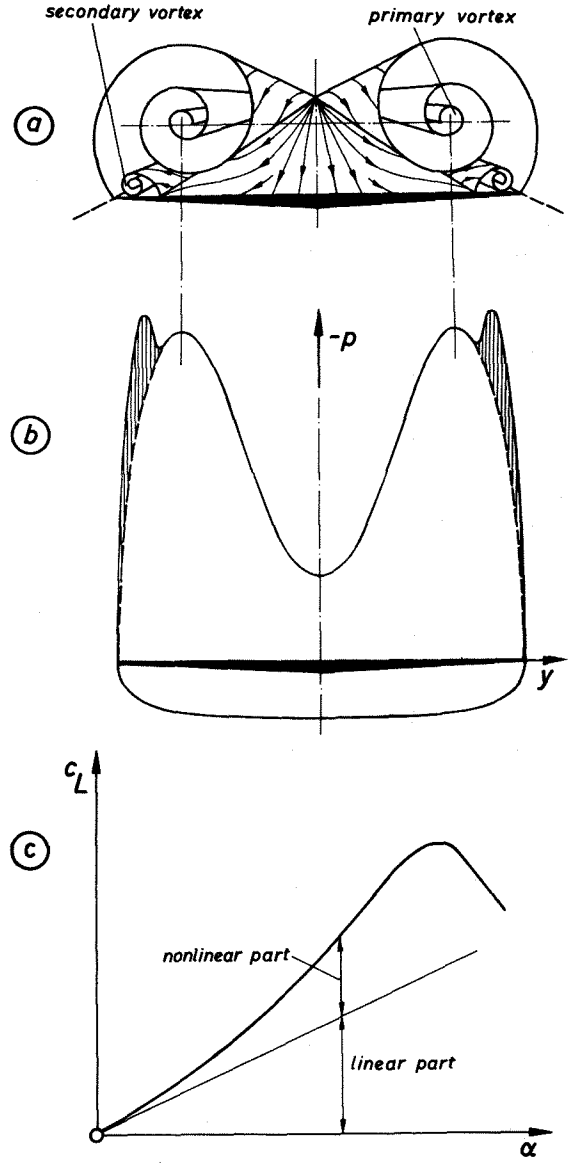

Fig.1: Flow over a slender sharp-edged wing (schematic)
a) Vortex formation
b) Pressure distribution
c) Lift characteristic

[+)] These investigations have been supported by public funds of the Federal Republic of Germany (Contract T/RF41/90010/91454)

[*] Dipl.-Ing. [**] Prof.Dr.-Ing.

of which is opposite to that of the corresponding leading-edge vortex. After these experimental results the flow over slender sharp-edged delta wings may be regarded as well understood. Present activities are aimed at a calculation of this flow in all details. Some progress has been achieved by F.T. Johnson, E.N. Tinoco [5] and O.A. Kandil [6,7], but some details of the theoretical approach are still subject to improvements. Recently a survey on the capability of various methods has been published by J.H.B. Smith [8].

For modern fighter aircraft wings with kinked leading-edges such as double-delta wings or strake-wings are mainly used. Some experimental investigations on wings of this shape by W.H. Wentz, M.C. McMahon [9,10], W. Staudacher [11], J.E. Lamar [12] and J.E. Lamar, J.M. Luckring [13] indicate that at low angles of attack two primary vortices are shed on each side of the wing, originating from the wing apex and from the leading-edge kink. Under certain conditions the two vortex systems merge into one system at increasing angle of attack. This process is a fundamental feature of the flow over wings with kinked leading-edges. It has not yet been analysed by comprehensive wind-tunnel tests and many details are not understood. On the other hand in theory only the method of K. Gersten [14] and the suction analogy [13] are available for application on double-delta wings. For a better representation of the real flow by a mathematical model there exists an urgent need for further experimental investigations to improve the physical understanding of the flow over double-delta wings.

Starting from the experience on vortex flows over delta wings according to D. Hummel [4] an experimental program on double-delta wings has been carried out at Institut für Strömungsmechanik of Technische Universität Braunschweig to analyse the flow and to provide a set of data for comparison with theoretical investigations. Some details have already been published by U. Brennenstuhl, D. Hummel [15,16] and following here a survey on the main results is given.

2. Notations

x,y,z	wing-fixed coordinates with origin at wing apex according to Fig.2
ξ,η	dimensionless wing-fixed coordinates ($\xi = x/c_i$, $\eta = y/y_1(x)$)
x_a,y_a,z_a	aerodynamic coordinates with origin at wing apex ($x_a = x\cos\alpha + z\sin\alpha$, $y_a = y$, $z_a = z\cos\alpha - x\sin\alpha$)
$\bar{y},\bar{z}$	aerodynamic coordinates in cross-sections x_a = const. with origin on the wing ($\bar{y} = y_a$, $\bar{z} = z_a + x_a\tan\alpha$)
$\bar{\xi},\bar{\eta},\bar{\zeta}$	dimensionless aerodynamic coordinates ($\bar{\xi} = x_a/c_i\cos\alpha$, $\bar{\eta} = \bar{y}/s$, $\bar{\zeta} = \bar{z}/s$)
x_K	distance of kink from wing apex
$y_1(x)$	local wing semi span
c_i	center-line chord of the wing
b	wing span ($b = 2s$)
s	wing half span ($s = b/2$)
d	wing thickness
γ	body half-angle according to Fig.2
ε	kink-angle according to Fig.2
S	wing area
A	wing aspect ratio ($A = b^2/S$)
U_∞	free stream velocity
$\vec{v}$	local velocity vector
$v_{\bar{\xi}},v_{\bar{\eta}},v_{\bar{\zeta}}$	components of $\vec{v}$ in the aerodynamic coordinate system
$v_{\bar{\eta}\bar{\zeta}}$	component of $\vec{v}$ in $\bar{\eta}/\bar{\zeta}$-plane ($v_{\bar{\eta}\bar{\zeta}} = \sqrt{v_{\bar{\eta}}^2 + v_{\bar{\zeta}}^2}$)
α	angle of attack
g	total pressure
p	static pressure
p_∞	free stream static pressure
q_∞	free stream dynamic pressure ($q_\infty = \rho V_\infty^2/2$)
c_g	total pressure coefficient ($c_g = (g-p_\infty)/q_\infty$)
c_p	static pressure coefficient ($c_p = (p-p_\infty)/q_\infty$)
c_L	lift coefficient ($c_L = L/Sq_\infty$)
ρ	density
ν	kinematic viscosity
Re	Reynoldsnumber ($Re = V_\infty c_i/\nu$).

3. Experimental set-up and program

3.1 Series of double-delta wings

The series of wings investigated at Institut für Strömungsmechanik of Technische Universität Braunschweig is shown in Fig.2. The wings I to VIII form

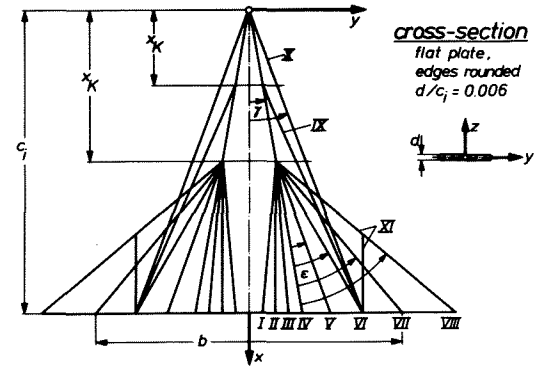

wing	I	II	III	IV	V	VI	VII	VIII	IX	X	XI
ε	-15°	-10°	-5°	0°	10°	20°	30°	40°	13.9°	0°	40°
γ	10°	10°	10°	10°	10°	10°	10°	10°	10°	20.7°	10°
b/c_i	0.18	0.18	0.26	0.35	0.54	0.75	1.02	1.37	0.75	0.75	0.75
x_K/c_i	0.50	0.50	0.50	0	0.50	0.50	0.50	0.50	0.25	0	0.50
A	0.28	0.23	0.45	0.71	1.31	2.05	3.01	4.35	1.74	1.50	1.62

Fig.2: Series of wings with kinked leading-edges

a subseries having the same front part with semi apex angle of $\gamma=10^{o}$ and the same kink position at $x_K/c_i=0.5$, where as the kink angle ε is varied from -15^{o} (wing I) up to $+40^{o}$ (wing VIII). Another subseries is formed by the wings VI, IX and X for which the wing span is kept constant and the kink position x_K/c_i is altered between $x_K/c_i=0.5$ (wing IV) and $x_K/c_i=0$ (delta wing X). Finally wing XI represents a modification of wing VIII with side-edges (cropped double-delta wing), the wing span being the same as for wings VI, IX and X. All wings were manufactured as thin flat plates having a thickness / chord ratio of $d/c_i=0.006$. All edges of the wings were rounded by a radius of half wing thickness. It turned out that this radius was small enough to produce leading-edge separation already at very small angles of attack. One set of wings having a chord length of $c_i=500$ mm has been produced for investigations in the 1.3 m wind-tunnel and another one having $c_i=140$ mm for the 0.33 m x 0.25 m water-tunnel of the Institut.

3.2 Description of the tests

All tests reported here have been carried out in the 1.3 m wind-tunnel of the Institut für Strömungsmechanik at Technische Universität Braunschweig. The Reynoldsnumber was $Re=1.3\cdot10^{6}$. In addition the flow over all wings has been visualized in the 0.33 m x 0.25 m water-tunnel of the Institut at $Re=10^{4}$. In the present context these investigations have been used only for comparison, and their results are not discussed in detail.

3.2.1 Balance measurements

For all wings three-component measurements have been carried out in the $-6^{o}\leq\alpha\leq+42^{o}$ angle of attack range. Some results have been published by U. Brennenstuhl, D. Hummel [15].

3.2.2 Surface oilflow patterns

The flow on the upper surface of all wings has been studied by means of oilflow patterns in order to obtain a general view of the vortex formation over the wings. For this purpose the wing surface was covered by a thin leaf of black synthetics which was painted by a mixture of aluminiumoxide-powder and petroleum and benzine (ratio of components: 1 g aluminiumoxide: 3 cm^3 petroleum: 1 cm^3 benzine) and exposed to the flow for about half a minute. Some oilflow patterns of this kind have been published in [15] and [16].

3.2.3 Pressure distributions

Three wings have been equipped with holes for surface pressure measurements in a few sections perpendicular to the free stream direction. The wing V and VII had one section at $x/c_i=0.75$, by which a study of the variation of the pressure distribution in this section with increasing angle of attack has been made possible. On wing VI the holes have been arranged in sections $x/c_i=0.375/0.500/0.625/0.750/0.875$, which allowed to investigate the pressure distribution in different sections at constant angle of attack.

3.2.4 Flow field measurements

Within the wing series, investigated here, wing VI has a central position. This wing belongs to the subseries in which the kink angle ε is varied as well as to the subseries in which the kink position x_K/c_i is altered. Fortunately this wing showed the most interesting flow phenomena, and therefore this wing was chosen to investigate the flow in details by flow field measurements.

The flow field in the vicinity of the wing has been measured in 5 planes perpendicular to the free stream velocity at the stations

Plane:	①	②	③	④	⑤
ξ =	0.75	0.85	1.004	1.10	1.20

at 2 different angles of attack

$\alpha = 10^{o}$: Planes ③, ④ and ⑤

$\alpha = 12^{o}$: Planes ①, ②, ③ and ④

In these planes the magnitude and the direction of the local velocity vector $\vec{v}$ has been determined by a conical 5-holes probe with a diameter of 2 mm. This probe has been traversed in the planes $\bar{\xi}$ = const. at a fixed angle with respect to the free-stream velocity. Total pressure, static pressure and dynamic pressure as well as the flow direction have been determined from the calibration diagrams of the probe. From these data lines of constant total pressure coefficient c_g have been evaluated and the velocity vector has been split up into the component $v_{\bar{\xi}}$ perpendicular to the $\bar{\eta}/\bar{\zeta}$-plane and into the component $v_{\bar{\eta}\bar{\zeta}}$ in the $\bar{\eta}/\bar{\zeta}$-plane.

4. Results

4.1 Double-delta wing VI, A = 2.05

4.1.1 Upper surface flow

The flow pattern on the upper surface of wing VI is shown in Fig.3 for different angles of attack. At small angles of attack $\alpha\leq10^{o}$ two primary vortices are formed on each side of the wing. These vortices originate from the wing apex and from the leading-edge kink. Both vortices are accompanied by secondary separations, which are clearly indicated by their separation lines up to the trailing-edge of the wing. Downstream of the leading-edge kink the inner primary vortex is no longer fed with vorticity. The strength of the inner primary vortex is therefore constant or decreases slightly due to viscous effects. On the other hand the whole vorticity shed from the rear part of the leading-edge is fed into the outer primary vortex. Its strength increases downstream. The two primary vortices have the same sense of rotation and therefore exists a tendency to moving around each other. Since the outer vortex becomes much stronger than the inner one as the wing trailing-edge is approached, this tendency leads to an outward (and downward) movement of the inner vortex which is clearly indicated by the flow pattern at $\alpha=10^{o}$.

The flow pattern at $\alpha=12^{o}$ according to Fig.3 shows that the two primary vortices on each side of the wing merge over the wing. Due to the influence of the outer primary vortex, the strength of which increases downstream, the weaker inner primary vortex moves outwards and joins to the outer primary vortex. The secondary separation corresponding to the inner primary vortex disappears downstream of the leading-edge kink. At the wing trailing-edge only a single primary vortex can be identified which is accompanied by a secondary separation originally belonging to the outer primary vortex.

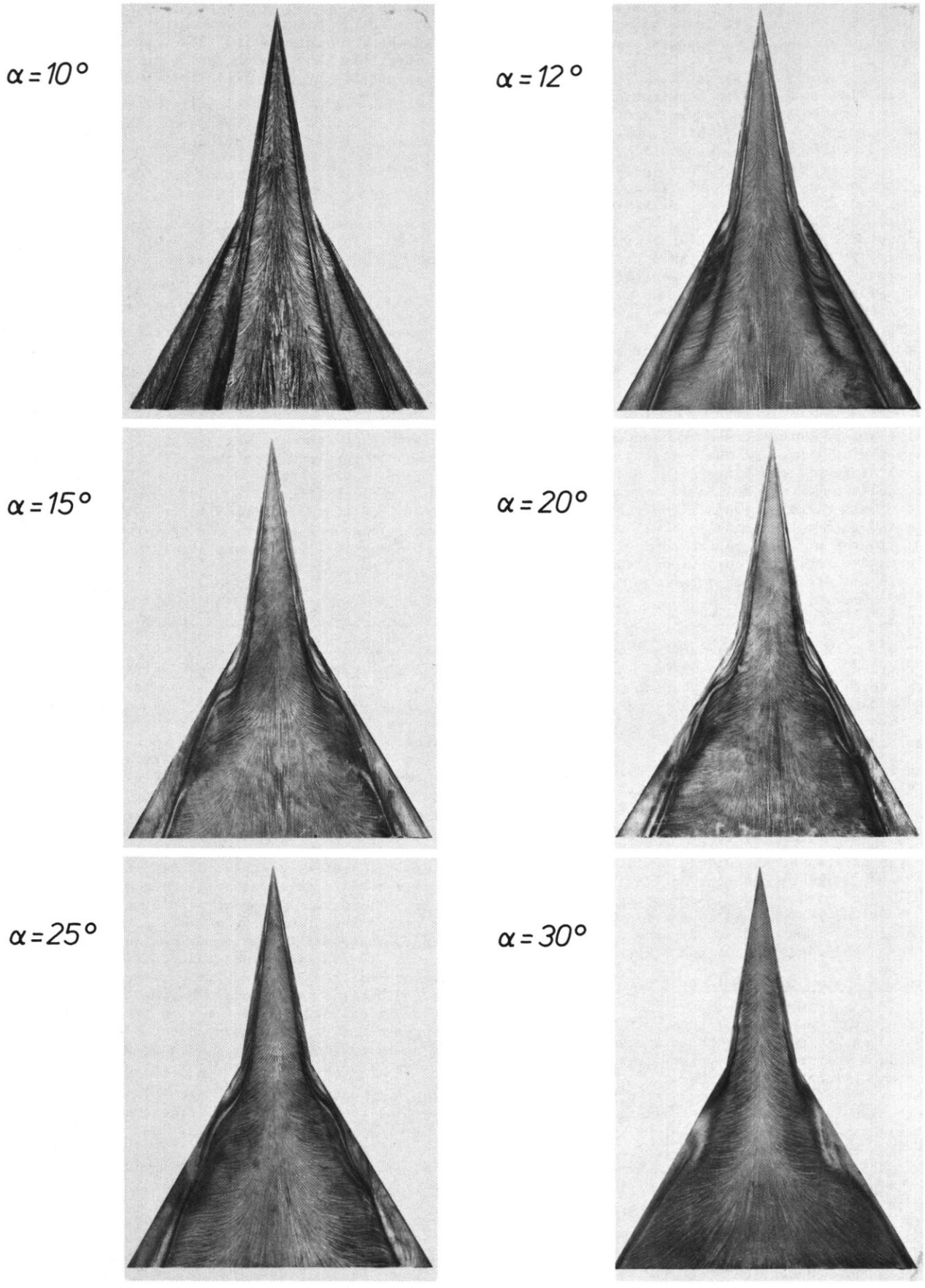

Fig.3: Flow pattern on the upper surface of wing VI at different angles of attack

With increasing angle of attack the "mixing length" of the two merging vortices decreases. At $\alpha=15^{o}$ two separate primary vortices are still present in the vicinity of the leading-edge kink, but for $x/c_i > 0,8$ a joined primary vortex is clearly indicated. At $\alpha=20^{o}$ two separate primary vortices can hardly be distinguished from the flow pattern in Fig.3. This means that the inner primary vortex now follows the leading-edge slope at the kink. It must be kept in mind, however, that the increment of vorticity is augmented abruptly at the leading-edge kink. The corresponding changes in the pressure distribution cause the wave-shaped slope of the secondary separation line.

Water-tunnel studies have shown, that vortex breakdown occurs within the joined vortices and that the breakdown point reaches the wing trailing-edge at $\alpha \approx 25^{o}$. The flow pattern for $\alpha=25^{o}$ according to Fig.3 shows not yet a significant effect of vortex breakdown. At $\alpha=30^{o}$ vortex breakdown takes place over the wing at $x/c_i \approx 0,6$. Downstream of this position the reduction of the suction peaks due to vortex breakdown is indicated by the shift of the secondary separation line towards the leading-edge according to D. Hummel [17]. The flow pattern at $\alpha=30^{o}$ is slightly unsymmetrical due to the fact that the position of vortex breakdown is very sensitive to small angles of sideslip; see e.g. D. Hummel, G. Redeker [18].

4.1.2 Pressure distribution

In order to study the merging process of the two primary vortices in more detail Fig.4 shows pressure distributions on the upper surface of the wing in a fixed section at $x/c_i=0.75$ for different angles of attack. This means that the various flow situations, discussed so far, occur in this section successively with increasing angle of attack.

At $\alpha=12^{o}$ two primary vortices are present at $x/c_i=0.75$. The strong outer vortex induces high suction and the corresponding secondary separation is clearly indicated. The weak inner vortex leads only to a smaller suction and its secondary separation - if present at all - is rather tiny. At $\alpha=15^{o}$ the section under consideration lies in the merging region . The two suction peaks induced by the two vortices, can clearly be identified. Due to the larger angle of attack the suction level is higher than at $\alpha=12^{o}$, but it is a remarkable fact that the suction due to the inner vortex has increased very much whereas the suction due to the outer vortex remained constant as compared to $\alpha=12^{o}$. Correspondingly the positions of both vortices have changed in spanwise direction. Both peculiarities of the pressure distribution at $\alpha=15^{o}$ in comparison with that at $\alpha=12^{o}$ lead to the conclusion that due to the mutual inductions between both vortices the inner vortex has moved outwards and downwards and the outer-vortex inward and upwards. Apart from the different vortex strengths the suction level induced by each vortex is governed by its distance from the wing surface and the position of the suction peak marks the spanwise location of the vortex. Between both vortices no pressure rise in flow direction is present and therefore no secondary flow separation is observed in this region.

At $\alpha=25^{o}$ the station $x/c_i=0.75$ lies in the region of the joined vortex upstream of the vortex breakdown point. The vortex induces a very high suction peak. The steep pressure rise towards the leading-edge leads to a distinctly marked secondary separation. At $\alpha=30^{o}$ vortex breakdown occurs upstream of the section $x/c_i=0.75$ under consideration. The measured pressure distribution shows the enlargement of the suction area in spanwise direction and the considerable reduction of the

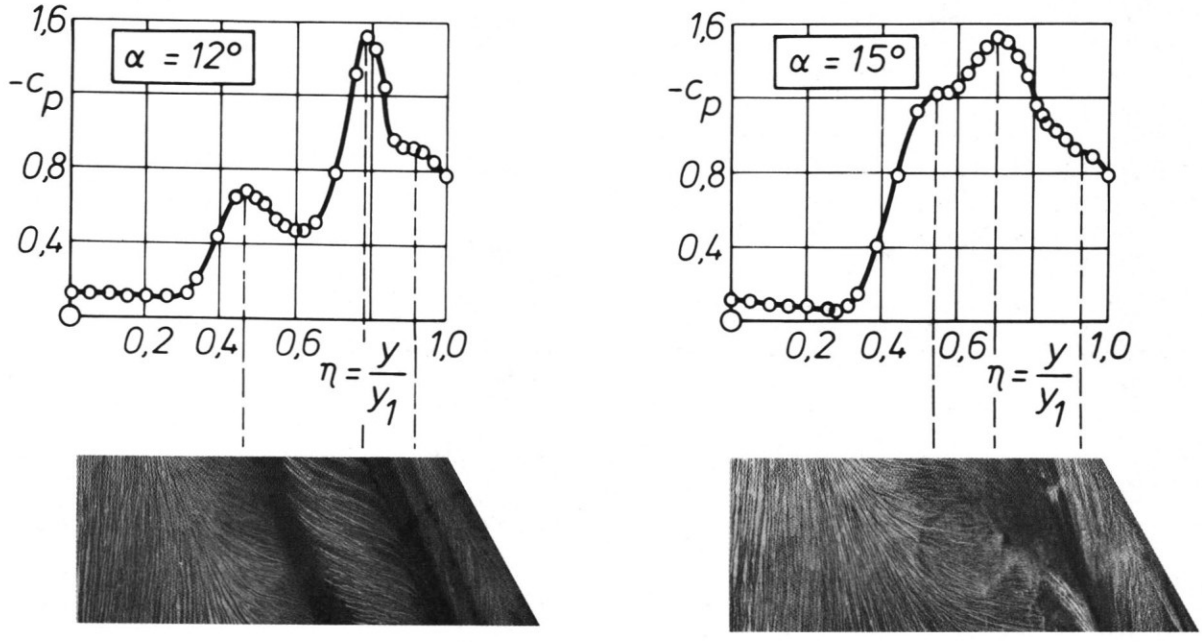

Fig.4: Pressure distributions and correlation to the flow pattern on the upper surface of wing VI at $x/c_i=0.75$ at different angles of attack

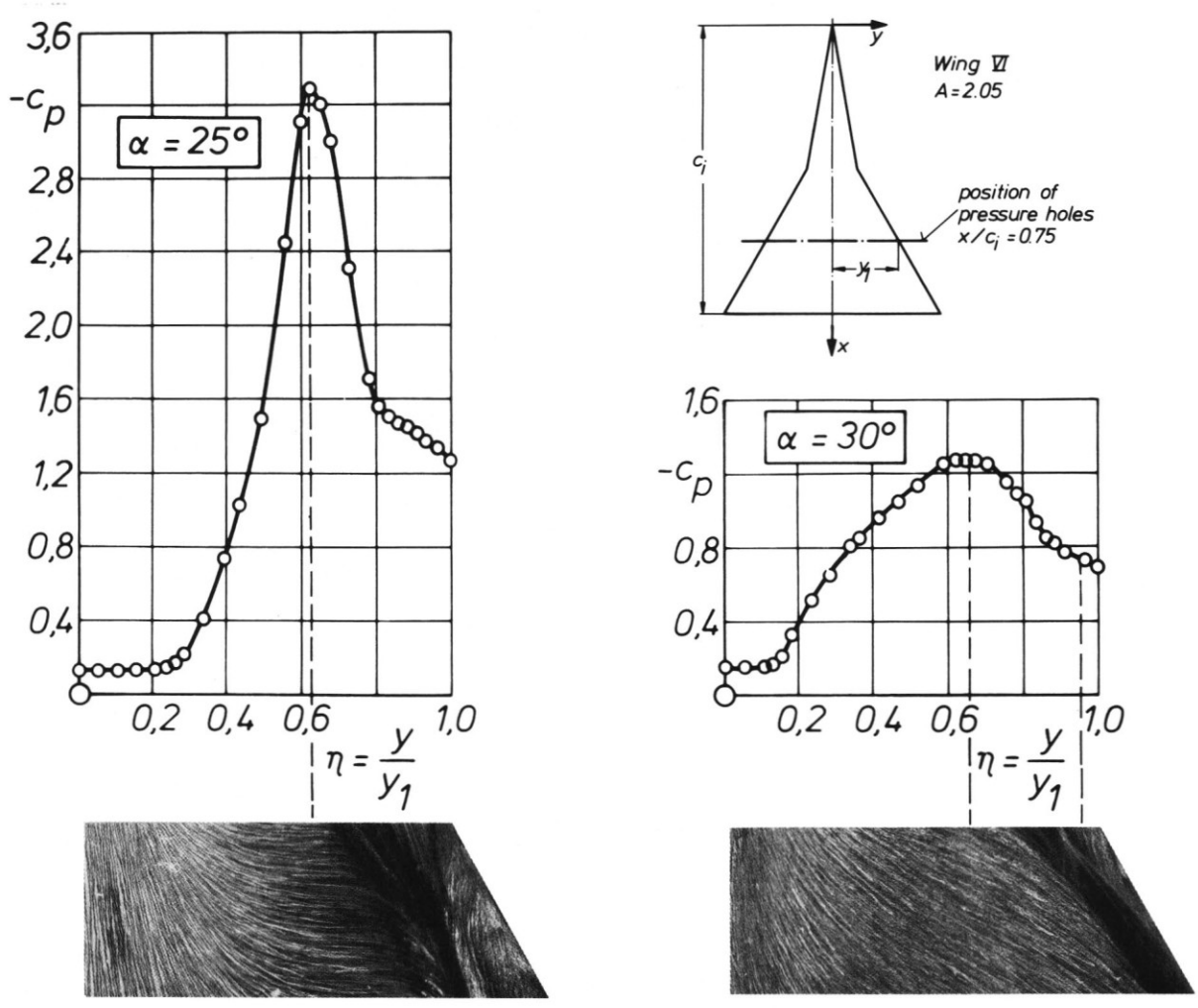

Fig.4 (contd.): Pressure distributions and correlation to the flow pattern on the upper surface of wing VI at $x/c_i = 0.75$ at different angles of attack

suction peak as well known from delta wings, see e.g. D. Hummel [19]. The pressure gradient towards the leading-edge is reduced and therefore the secondary separation line is situated closer to the leading-edge as compared to the situation at $\alpha=25^o$.

4.1.3 Flow field

A typical result of the flow field measurements on wing VI at $\alpha=10^o$ is shown in Fig.5. In this case according to Fig.3 two primary vortices are shed on each side of the wing. The plane of the measurements is located a short distance downstream of the wing trailing-edge at $\bar{\xi}=1.10$. The total pressure contours in Fig.5a clearly mark the centres of the inner and of the outer primary vortex. The inner vortex is the weaker one as indicated by the smaller size of the area of total pressure losses and by the lower peak value of these losses. Due to the mutual interference of the two vortices the inner vortex has a smaller distance from the wing plane as already discussed with respect to Fig.3. The vortex sheets are marked by relative minima of total pressure. Their positions are indicated in Fig.5 by dash-dotted lines. The trailing vortex sheet, which is clearly indicated by a small band of total pressure losses in spanwise direction, is considerably warped up in the outer region, $\bar{\eta} > 0.7$, and forms a concentrated trailing-vortex at $\bar{\eta} = 0.92$, $\bar{\zeta} = 0.09$, the rotation of which is opposite to that of the outer leading-edge vortex. Such a concentrated trailing-vortex is well known for delta wings according to D. Hummel [4] . It starts at the trailing-edge of the wing in the vicinity of the pressure minimum and its strength increases downstream. In the outermost part of the wing span the trailing vortex sheet and the leading-edge vortex sheet of the outer primary vortex are connected and it is this part of the flow field where the remains of the outer secondary separation are found by relatively low values of total pressure. The flow field of the outer primary vortex is quite similar to that of the vortex over and behind a simple delta wing. In the vicinity of the inner vortex the trailing vortex sheet is also distinctly warped but a concentrated counter-rotating trailing vortex could not be identified confidently. The counter rotating trailing vorticity is relatively weak in this region. Other problems arise with the interpretation of the secondary separation in connection with the inner primary vortex. The secondary vortex is relatively strong as compared to the secondary vortex corresponding to the outer primary vortex, and its

a) Lines of constant total pressure coefficient, $c_g = (g-p_\infty)/q_\infty = \text{const.}$

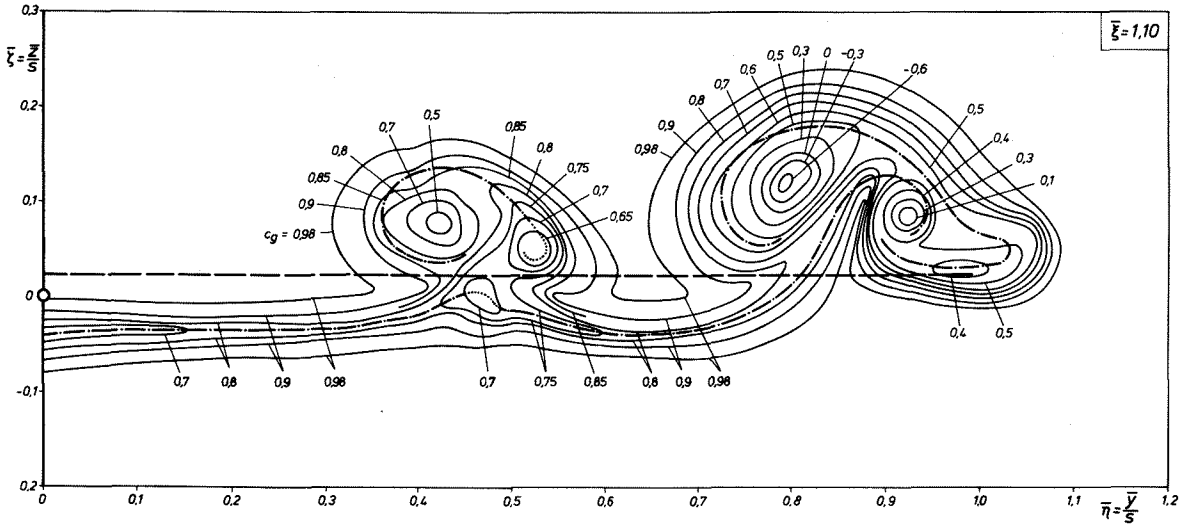

b) Component $v_{\bar{\eta}\bar{\zeta}}$ of the velocity vector in the $\bar{\eta}/\bar{\zeta}$-plane ⟵ $|v_{\bar{\eta}\bar{\zeta}}/U_\infty| = 1$

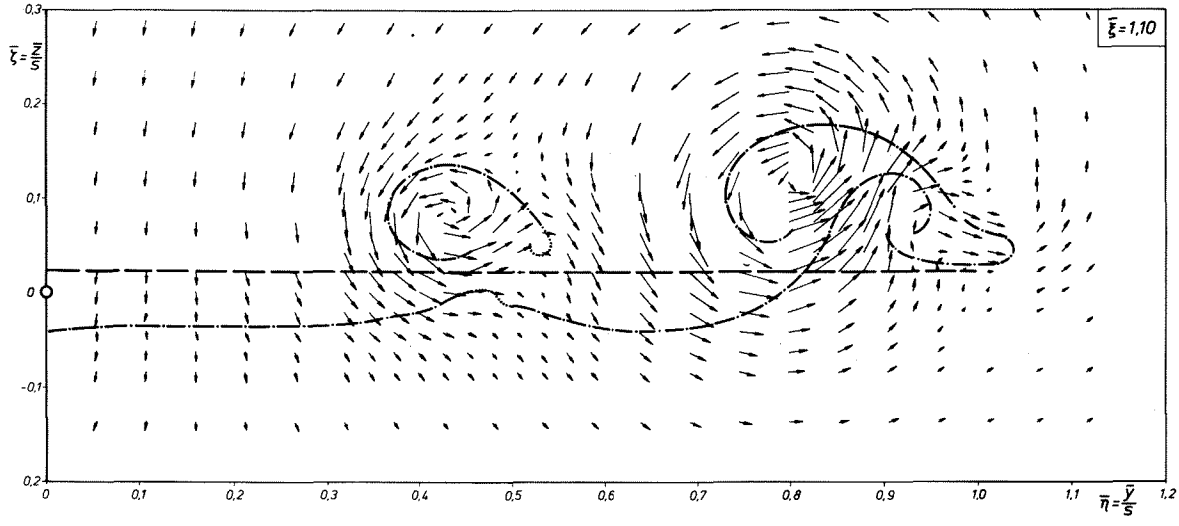

Fig.5: Vortex formation behind wing VI in plane (4) ($\bar{\xi}$=1.10) at $\alpha=10^o$

— — — — trailing-edge —·—·— vortex sheet

distance from the wing plane is large. On the other hand the vortex sheet which forms the inner primary vortex must have a free end, originating from the leading-edge kink, since vorticity is no longer shed into the inner vortex beyond that point. The free end of the vortex sheet should have a tendency to rolling up in the same sense as the inner vortex. There might exist a connection between the free end of the vortex sheet and the secondary vortex. These details of the flow are presently not yet fully understood and further studies on a larger wind-tunnel model are in progress by this time.

The vectors of the velocity component $v_{\bar{\eta}\bar{\zeta}}$ in the $\bar{\eta}/\bar{\zeta}$-plane are shown in Fig.5b. The two primary vortices as well as the concentrated trailing vortex corresponding to the outer primary vortex are clearly to identify. Between the two primary vortices a stagnation region is formed in the plane of measurements. This stagnation region is located close to the inner primary vortex indicating this vortex to be the weaker one. The vortex sheets must be tangential with the local flow direction. The cross flow components which appear in Fig.5b at the vortex sheets are due to the fact that the vortex sheets are not perpendicular to the $\bar{\eta}/\bar{\zeta}$-plane. In order to verify the tangential flow condition the component $v_{\bar{\xi}}$ has to be added perpendicular to the $\bar{\eta}/\bar{\zeta}$-plane and the resulting local velocity vector $\vec{v}$ is then tangential with the vortex sheet. Far away from the origin $\bar{\eta}=\bar{\zeta}=0$ the arrows tend to zero, since the free stream velocity U_∞ has no component in the $\bar{\eta}/\bar{\zeta}$-plane.

According to Fig.3 at $\alpha=12^o$ the merging process of the two primary vortices takes place over the wing VI. In order to get a first insight into this flow field the positions of the axes of both vortices have been determined by moving the probe into the corresponding total pressure minimum. The result is shown in Fig.6. The spanwise position of the vortex axes may be taken from the left-hand diagram, whereas in the right-hand figure the vortex centres have been drawn for seven

cross-planes (ⓐ to ⓖ) in correct scale with respect to the local half span of the wing. It turns out that due to the mutual interference of the two vortices the inner vortex moves downwards and outwards and the outer vortex moves inward and upwards. Downstream of the leading-edge kink the movement of the vortex axes is small at first. As the strenght of the outer vortex increases the movement of the weaker inner vortex is augmented and finally the inner vortex is merged into the outer vortex at a very short distance in chordwise direction. This abrupt merging is due to the increasing strength of the outer vortex and the decreasing distance between the two vortices in the course of the merging process. The inner primary vortex could be identified by a separate total pressure minimum until its axis was located beneath the axis of the outer primary vortex.

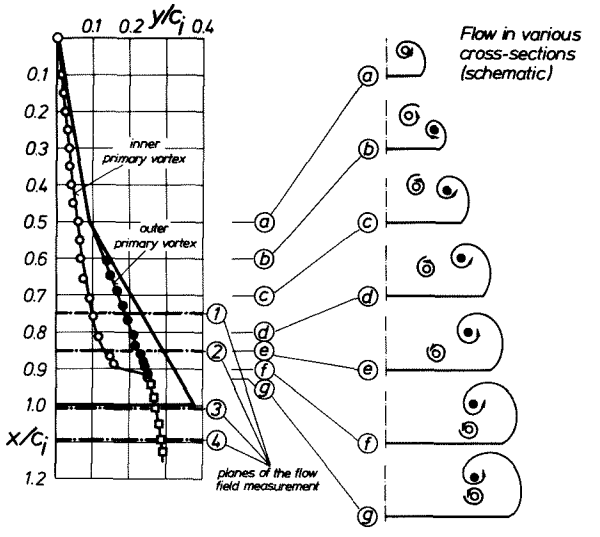

Fig.6: Position of the vortex axes at the merging process of the primary vortices on wing VI at $\alpha=12^{o}$.

- O Axis of the inner vortex
- ● Axis of the outer vortex
- □ Axis of the joined vortex

The merging process of the two primary vortices has been studied on wing VI at $\alpha = 12^{o}$ by flow field measurements in 4 planes as indicated in Fig.6. The planes ① and ② were located in a region where two separate vortex centres are still present, whereas in the planes ③ and ④ a single joined vortex appears.

The total pressure contours in the four planes are shown in Fig.7. In plane ① at $\bar{\xi}=0.75$ the outer primary vortex has grown up to about the size of the inner vortex. Both vortices have about the same distance from the surface of the wing, but the outer vortex is already stronger than the inner one, which can indirectly be taken from the total pressure minima of $c_g=+0.3$ in the inner vortex and $c_g=-0.7$ in the outer vortex. The secondary separation corresponding to the outer primary vortex is indicated by low values of total pressure near the leading-edge, whereas a secondary vortex related to the inner primary vortex cannot be detected. The areas of total pressure losses of both vortices are already connected and as a first interference effect between both vortices the vortex sheet of the inner vortex is implicated in the outer primary vortex. In plane ② at $\bar{\xi}=0.85$ the downward and outward movement of the inner vortex is clearly marked as compared to plane ①. The vortex sheet of the inner vortex could be detected underneath the axis of the outer vortex as a long, curved line. The present result is in good agreement with the measured pressure distributions and their interpretation according to Fig.4. In plane ③ at $\bar{\xi}=1.004$ a single joined primary vortex is present having a very complicated structure in detail. The absolute total pressure minimum of $c_g<-0.6$ can easily be identified as the centre of the outer primary vortex. But within the flow field another (relative) minimum of total pressure coefficient $c_g=0.3$ is found at $\bar{\eta}=0.79$, $\bar{\zeta}=0.14$, which must be regarded from its magnitude and from its position as the center of the inner primary vortex. Beyond that also some remains of the vortex sheet of the inner vortex could be identified within the joined vortex. The secondary separation close to the leading edge is indicated by high total pressure losses close to the wing surface. Plane ③ is located slightly downstream of the trailing-edge of the wing. At about $\bar{\eta}=0.75$ the trailing vortex sheet is already distinctly warped, which indicates the onset of the concentrated trailing vortex. It is interesting to note, that the trailing vortex corresponding to the joined vortex starts between the centres of the two original vortices. Plane ④ at $\bar{\xi}=1.10$ is located downstream of the trailing-edge of the wing. Within the joined vortex the total pressure losses of both original vortices have merged, forming a total pressure minimum of $c_g<-0.9$. The counter rotating trailing vortex is distinctly marked and the secondary vortex is implicated into this trailing vortex. A comparison of the total pressure contours in all 4 planes shows the increase of the vortex sheets thickness in downstream direction. This is due to the fact that the region of total pressure losses widens perpendicular to the flow direction due to viscous effects.

The components $v_{\bar{\eta}\bar{\zeta}}$ of the local velocity vector are shown in Fig.8 for all 4 planes. The two primary vortices as well as the counter-rotating trailing vortex are clearly indicated by the flow directions and by increasing velocities towards their centres. At the vortex sheets, especially at that of the inner primary vortex, considerable crossflow components are observed. This is an outcome of the fact that these vortex sheets are strongly inclined with respect to the planes of the measurements. In the two planes over the wing underneath the two vortices large velocity components occur. On the one hand the strong outer vortex induces high outward velocities there. On the other hand the axis of the inner vortex is considerably inclined against the planes of the measurements according to Fig.6 and therefore not only the circumferential component but also a large portion of the axial velocity component of the inner vortex is noticed in the planes of the measurements.

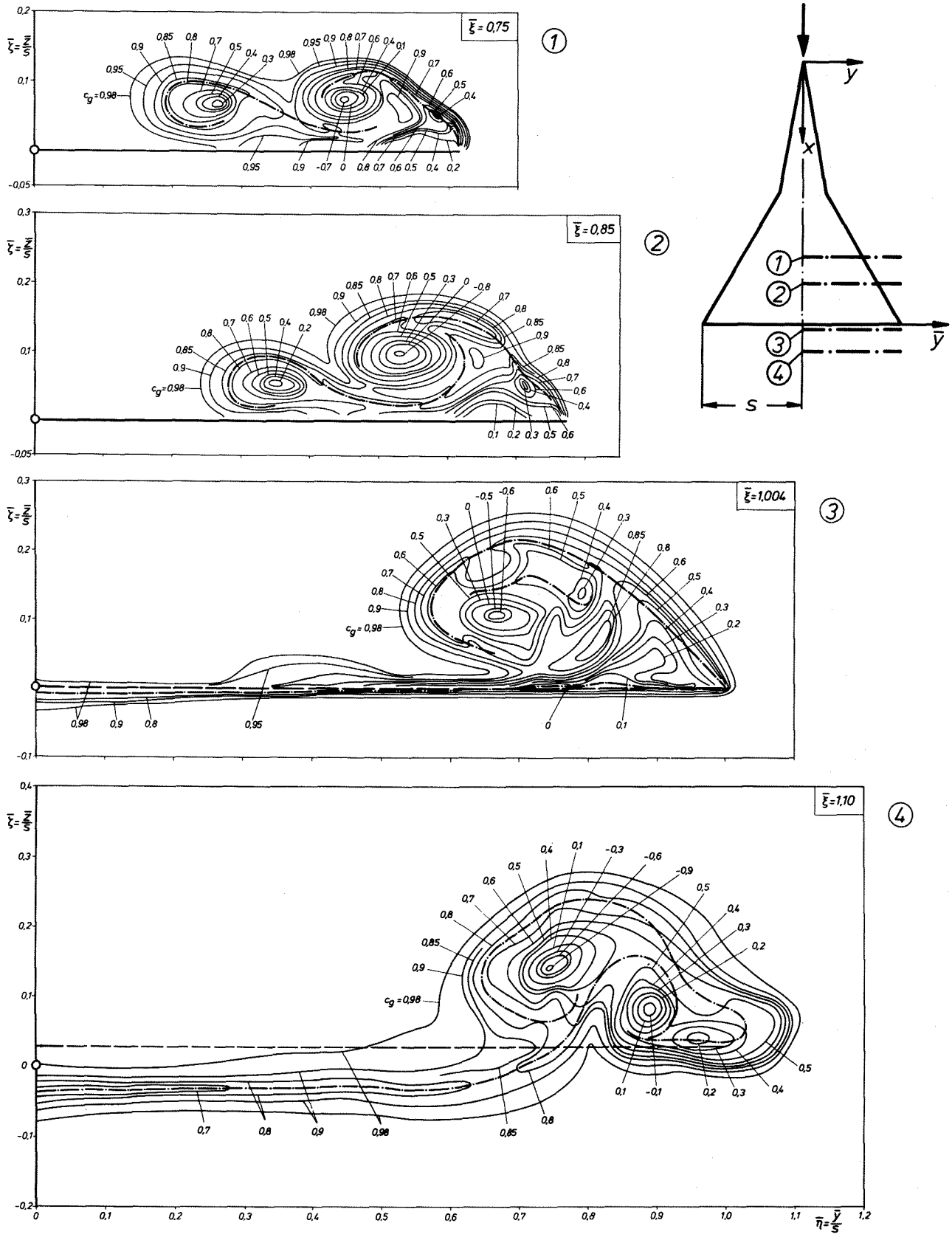

Fig.7: Distribution of total pressure in four planes over and behind wing VI at $\alpha=12^{o}$. Lines of constant total pressure coefficient, $c_g=(g-p_\infty)/q_\infty=\text{const}$.

——— wing — · — · — vortex sheet

— — — trailing-edge

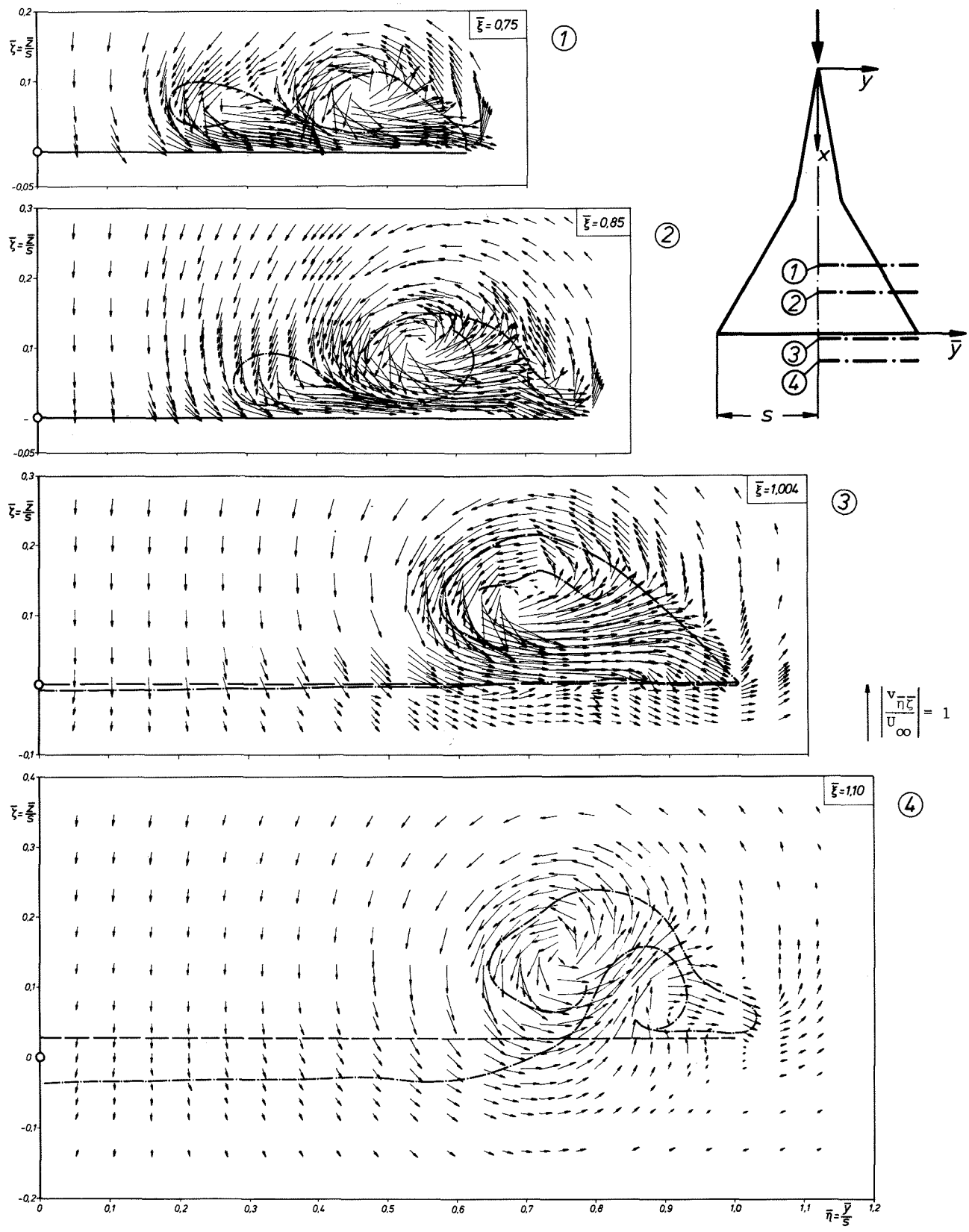

Fig.8: Flow field in four planes over and behind wing VI at $\alpha=12^{o}$. Component $v_{\eta\zeta}$ of the velocity vector $\vec{v}$ in the $\bar{\eta}/\bar{\zeta}$-plane.

wing — vortex sheet

trailing-edge

4.1.4 Forces and moments

The lift and pitching moment characteristics of wing VI in symmetrical flow are shown in Fig.9. Due to the vortex formation over the wing nonlinear lift and pitching moment curves turn out. At $\alpha \approx 11^{\circ}$ the junction of the two primary vortices is already finished at the trailing-edge. At the same angle of attack the lift and pitching moment characteristics show a distinctly marked kink. At angles of attack $\alpha > 11^{\circ}$ the slope of lift is smaller and the correspondingly reduced slope of the nose-down pitching moment indicates that a certain loss of lift has taken place in the rear part of the wing. The explanation for these changes in the aerodynamic coefficients is the fact that the spanwise integral over the pressure distribution in the region of the joined vortex is smaller than the integral over a pressure distribution with two suction peaks in the region of two separate primary vortices. This means that wings with two separate primary vortices on each half wing produce a large nonlinear contribution to the aerodynamic coefficients, but if these vortices merge and form a single joined vortex the nonlinearity in the aerodynamic characteristics is distinctly reduced. At $\alpha \approx 26^{\circ}$ vortex breakdown appears in the joined vortices at the trailing-edge of the wing and moves upstream over the wing with increasing angle of attack. This leads to the well known reduction of lift and of nose-down pitching moment. Observations of the flow in the water-tunnel have shown that up to $\alpha = 40^{\circ}$ the vortex breakdown point did not pass the leading-edge kink position $x_K/c_i = 0.5$. This means that up to this angle of attack a sound vortex formation takes place in the highly swept front part of the wing. The slope of the aerodynamic coefficients at angles of attack $\alpha > 26^{\circ}$ is therefore due to modifications of the pressure distribution on the rear part of the wing. In this angle of attack range the type of flow changes there from a vortex without breakdown over a vortex with breakdown in which the instationary flow is still embedded in a sound outer vortex flow, up to a completely instationary dead-water region over the whole rear part of the wing. Detailed investigations of these flow phenomena are in progress at present and therefore final results are not yet discussed here.

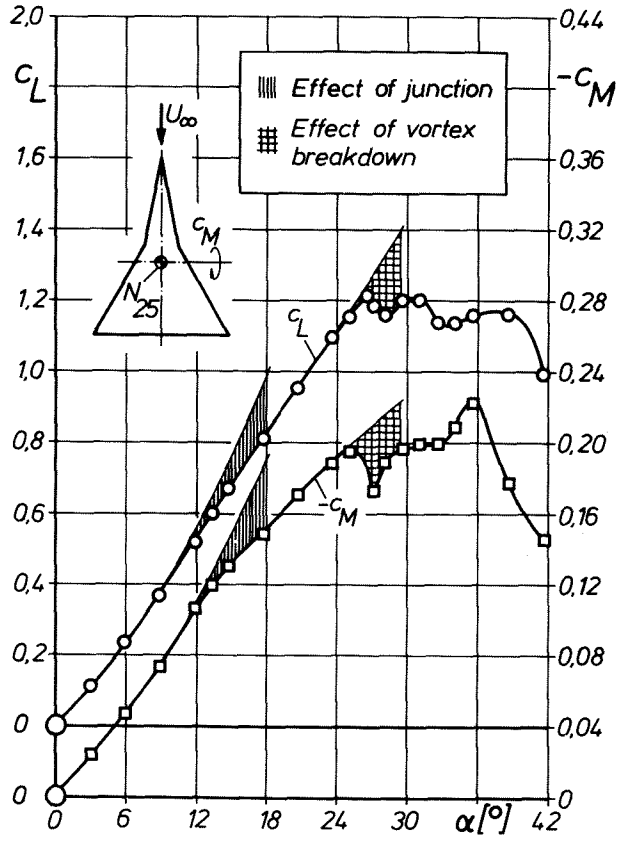

Fig.9: Lift and pitching moment characteristics of wing VI

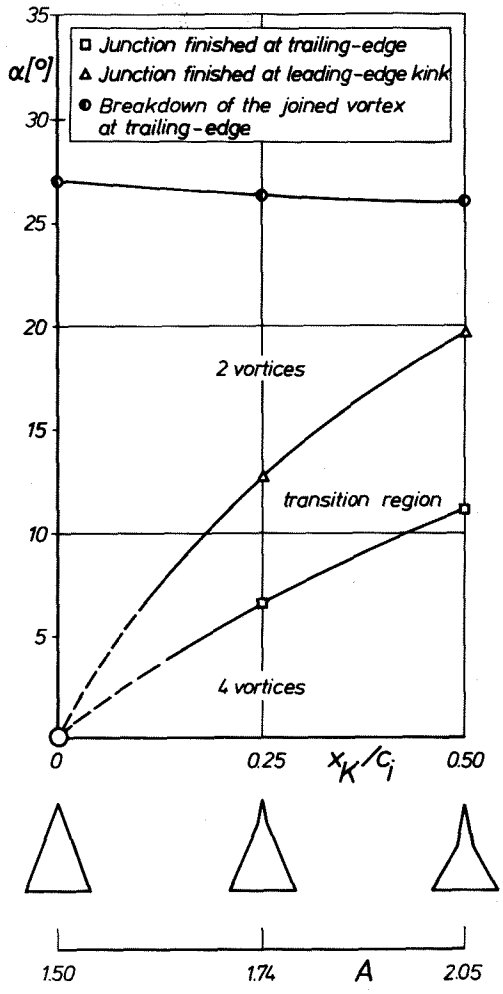

Fig.10: Vortex formation over double-delta wings with different leading-edge kink positions x_K/c_i at various angles of attack α (constant parameters $\gamma = 10^{\circ}$, $b/c_i = 0.75$).

4.2 Influence of kink position x_K/c_i

Within the series of double-delta wings according to Fig.2 the wings VI, IX and X form a subseries in which the leading-edge kink position x_K/c_i is the varied parameter at fixed span/chord ratio b/c_i. The vortex formation on this subseries of wings is summarized in Fig.10 according to U. Brennenstuhl, D. Hummel [15]. The series starts

with a simple delta wing at $x_K/c_i=0$ having a two-vortex system (one vortex on each half wing) over the upper surface. The basic flow pattern for all wings with kinked leading-edges ($\varepsilon>0$) at small angles of attack is a four-vortex system. At very low angles of attack the merging process takes place downstream of the wing trailing-edge thus having no significant influence on the wing. With increasing angle of attack the point where the junction of the two vortices of each wing half is finished moves upstream and reaches the wing trailing-edge at a certain angle of attack, which is marked in Fig.10. At further increasing angle of attack the point of finished junction moves upstream and reaches the leading-edge kink at another distinct value of α which is also drawn in Fig.10. At this angle of attack the last remains of the original four-vortex system disappear and at still larger angles of attack a two-vortex system is present. With increasing distance of the leading-edge kink from the wing apex the onset of these phenomena is shifted towards higher angles of attack. This is due to the fact that with increasing x_K/c_i at constant b/c_i the leading-edge kink angle ε is enlarged and the distance between the vortices is augmented. A merging process is then only possible at increased vortex strengths which are present at higher angles of attack.

At large angles of attack vortex breakdown occurs in the joined vortices and the breakdown point crosses the trailing-edge of the wing at a certain angle of attack which is also marked in Fig.10. This special angle of attack decreases only slightly with increasing parameter x_K/c_i. This behaviour might be the outcome of two effects which cancel largely: On the one hand the angle of sweep-back of the outer part of the wing decreases with increasing parameter x_K/c_i and if the results for delta wings e.g. after D. Hummel, P.S. Srinivasan [20] are applied, this should reduce the value of the angle of attack at which vortex breakdown occurs at the wing trailing-edge. On the other hand the length of the highly swept front part of the wing increases with increasing parameter x_K/c_i. Therefore at the leading-edge kink an inner primary vortex is present the strength of which increases with the parameter x_K/c_i. This vortex follows the leading-edge at the kink and its initial conditions at the kink lead to a considerable stabilizing effect with respect to vortex breakdown as compared with a simple delta wing having the same leading-edge sweep. It turns out that wings with constant b/c_i and different leading-edge shapes have similar vortex breakdown characteristics.

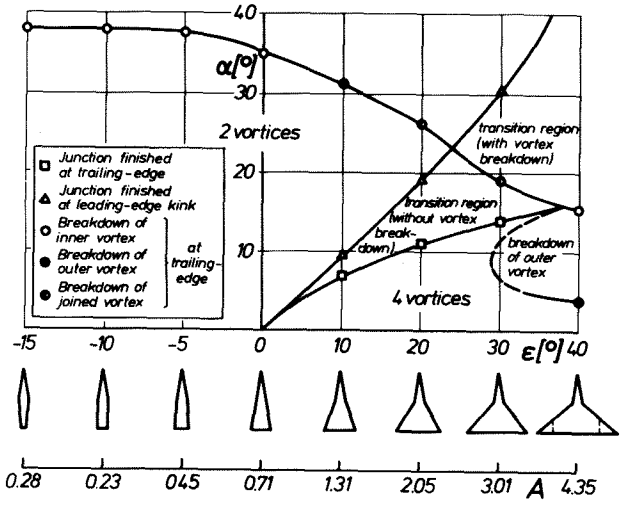

Fig.11: Vortex formation over double-delta wings with different leading-edge kink angles ε at various angles of attack α. (Constant parameters $x_K/c_i=0.5$, $\gamma=10^o$)

4.3 Influence of leading-edge kink angle ε

Within the investigated wing series according to Fig.2 the wings I to VIII form a subseries in which the leading-edge kink angle ε is the varied parameter at fixed front part body angle $\gamma=10^o$ and fixed kink position $x_K/c_i=0.5$. The vortex formation on this subseries of wings is summarized in Fig.11 according to U. Brennenstuhl, D. Hummel [16]. At leading-edge kink angles $\varepsilon\leq 0^o$ a two-vortex system is formed over the wings at any angle of attack. Due to the very low aspect ratio of these wings vortex breakdown occurs over the wing only at very high angles of attack. For positive leading-edge kink angles $\varepsilon>0^o$ at small angles of attack a four-vortex system is the basic flow pattern over the wing. At a certain angle of attack, the value of which increases with increasing kink angle ε, the junction of the two vortices on each wing half is finished at the wing trailing-edge. At a higher angle of attack the junction is finished already at the leading-edge kink. At this angle of attack the last remains of the original four-vortex system disappear and at still larger angles of attack a two vortex-system is present. At very high angles of attack vortex breakdown occurs within the joined vortices. The value of the angle of attack, at which the vortex breakdown point crosses the trailing-edge of the wing, reduces considerably with increasing kink angle ε due to the increasing aspect ratio of the wings. Up to wing VI ($\varepsilon=20^o$) the four-vortex system has completely disappeared before vortex breakdown of the joined vortices occured over the wing.

At very high kink angles ε the two primary vortices on each half wing are located at a large distance from each other. For wing VIII ($\varepsilon=40^o$) it was found that with increasing angle of attack vortex breakdown occured at a low angle of attack in the outer primary vortex and at a higher angle of attack also in the inner primary vortex. This means that in this case the four-vortex system is destroyed by vortex breakdown before a merging process of the primary vortices takes place. This behaviour of wing VIII must be regarded as the limiting case for high kink angles ε.

For $20^o<\varepsilon<40^o$ rather complicated flow phenomena have been found. At $\varepsilon=25^o$ (this wing was not included in the wing series investigated here) one should expect that a merging process of the primary vortices takes place over the wing at $\alpha>13^o$ and that vortex breakdown in the joined vortex occurs over the wing before the junction has reached the leading-edge kink. This means that e.g. at $\alpha=20^o$ downstream of the kink at first two primary vortices are present on each half wing which merge then into a single vortex which is subject to vortex breakdown before the trailing-edge is reached. The flow pattern which has been observed on wing VII ($\varepsilon=30^o$) is still more complicated. At small angles of attack the behaviour which is typical for high kink angles ε has been observed: vortex breakdown occured in

the outer primary vortex at a relatively low angle of attack. At increasing angle of attack the interference between the sound, unbroken part of the outer primary vortex and the inner primary vortex led to a stabilization of the outer vortex and thus to a downstream movement of the breakdown point until vortex breakdown disappeared completely. At further increasing angle of attack the behaviour described for an $\varepsilon=25^{\circ}$ wing has been found on wing VII. The details of these flow phenomena need further investigations, but it is interesting to note that the merging process of the two primary vortices has a stabilizing effect with respect to vortex breakdown not only for the joined vortex but also for an already broken outer primary vortex.

4.4 Concluding remarks

It is quite obvious from the present investigations that the merging process of the two primary vortices on each side of double-delta wings is caused by their mutual interference. This process is governed by Biot-Savart's law and must be regarded to be a potential flow effect. For certain combinations of wing planform shape and angle of attack either a four-vortex system or a two-vortex system or a mixed system with a transition from four to two vortices exists over the wing. For a four-vortex system as well as for a transitional system quantitative experimental data may be taken from the present investigation.

5. Summary

A series of double-delta wings has been investigated in the 1.3 m low-speed wind-tunnel of the Institut für Strömungsmechanik at Technische Universität Braunschweig. Three-component, pressure distribution and flow field measurements as well as flow visualization at the wing's surface have been carried out at $Re=1.3\cdot10^{6}$.

At moderate positive leading-edge kink angles (wings V and VI) for small angles of attack two primary vortices exist on each side of the wing, originating from the apex and from the leading-edge kink of the wing. At increasing angles of attack these vortices merge and form a joined vortex. At a certain angle of attack the junction is finished at the leading-edge kink and all remains of the original system of two vortices on each side of the wing disappear. At higher angles of attack on each wing half only a single primary vortex is present, which follows the slope of the leading-edge at the kink. At very high angles of attack vortex breakdown occurs in the joined vortices which leads to the well-known limitations of the aerodynamic coefficients.

The flow field of wing VI ($A=2.05$, $\varepsilon=20^{\circ}$) has been analysed in detail. Quantitative results of probe measurements are given for a plane downstream of the trailing-edge at $\alpha=10^{\circ}$. In this case two primary vortices were present on each side of the wing and the outer one was accompanied by a counter-rotating trailing-vortex as known from delta wings. The merging process has been studied quantitatively by probe measurements in four planes over and behind the wing at $\alpha=12^{\circ}$ as well as by pressure distribution measurements at the wing surface. The weaker inner primary vortex moves downwards and outwards and the stronger outer primary vortex goes upwards and inward. Due to the increasing strength of the outer primary vortex the inner vortex joins the outer one quite rapidly. The merging process can be explaned by the mutual interference of the vortices and must be regarded to be a potential flow effect. Due to the junction of the primary vortices the nonlinear aerodynamic coefficients are distinctly reduced.

Considering all wings of the investigated series the influence of some important parameters could be analysed. A rearward movement of the leading-edge kink at constant wing span leads to a shift of the merging process of the two vortices to higher angles of attack. With increasing leading-edge kink angle ε the merging of the vortices also occurs at larger angles of attack. At very high kink angles the two vortices are destroyed successively by vortex breakdown before a merging process takes place and between both flow patterns a rather complicated transition region has been found.

6. References

[1] D. Küchemann: Die aerodynamische Entwicklung von schlanken Flügeln für den Überschallflug. Jb. 1962 d. WGLR, 66-77.

[2] J.H.B. Smith: A review of separation in steady, three-dimensional flow. AGARD-CPP-168-(1975), 31-1 to 31-17.

[3] D.J. Peake: Controlled and uncontrolled flow separation in three dimensions. NAE Aeron.Rep. LR-591 (1976).

[4] D. Hummel: On the vortex formation over a slender wing at large angles of incidence. AGARD-CPP-247 (1978), 15-1 to 15-17.

[5] F.T. Johnson, E.N. Tinoco: Recent advances in the solution of three-dimensional flows over wings with leading edge vortex separation. AIAA-Paper 79-282 (1979).

[6] O.A. Kandil: Numerical prediction of vortex cores from the leading and trailing edges of delta wings. ICAS-Paper 14.2., München 1980.

[7] O.A. Kandil: Recent improvements in the prediction of leading and trailing edge vortex cores of delta wings. AIAA-Paper 81-1263 (1981).

[8] J.H.B. Smith: Vortical flows and their computation. RAE Tech. Memo. Aero 1866 (1980).

[9] W.H. Wentz, M.C. Mc Mahon: An experimental investigation of the flow fields about delta and double-delta wings at low speeds. NASA CR-521 (1966).

[10] W.H. Wentz, M.C. Mc Mahon: Further experimental investigations of delta and double-delta wing flow fields at low speeds. NASA CR-714 (1967).

[11] W. Staudacher: Flügel mit kontrollierter Ablösung. Vortrag auf der 10. Jahrestagung der DGLR, Berlin 1977, DGLR-Vorabdruck 77-028.

[12] J.E. Lamar: Strake wing analysis and design. AIAA Paper 78-1201 (1978).

[13] J.E. Lamar, J.M. Luckring: Recent theoretical developments and experimental studies pertinent to vortex flow aerodynamics - with a view towards design.
AGARD-CPP-247 (1978), 24-1 to 24-31.

[14] K. Gersten: Nichtlineare Tragflächentheorie, insbesondere für Flügel mit kleinem Seitenverhältnis.
Ing.Arch. 30 (1961), 431-452.

[15] U. Brennenstuhl, D. Hummel: Untersuchungen über die Wirbelbildung an Flügeln mit geknickten Vorderkanten.
Z.Flugwiss. Weltraumforsch. 5 (1981), 375-381.

[16] U. Brennenstuhl, D. Hummel: Weitere Untersuchungen über die Wirbelbildung an Flügeln mit geknickten Vorderkanten.
Vortrag DGLR-Symposium "Strömungen mit Ablösung", Stuttgart, 23.-25.11.1981, DGLR-Vorabdruck 81-256 (1981).

[17] D. Hummel: Experimentelle Untersuchung der Strömung auf der Saugseite eines schlanken Deltaflügels.
Z.Flugwiss. 13 (1965), 247-252.

[18] D. Hummel, G. Redeker: Über den Einfluß des Aufplatzens der Wirbel auf die aerodynamischen Beiwerte von Deltaflügeln mit kleinem Seitenverhältnis beim Schiebeflug.
Jb. 1967 der WGLR, 232-240.

[19] D. Hummel: Zur Umströmung scharfkantiger schlanker Deltaflügel bei großen Anstellwinkeln.
Z.Flugwiss. 15 (1967), 376-385.

[20] D. Hummel, P.S. Srinivasan: Vortex breakdown effects on the low-speed aerodynamic characteristics of slender delta wings in symmetrical flow.
J.Roy.Aeron.Soc.71 (1967), 319-322.